Vol. 62: 173–188, 2015
doi: 10.3354/cr01256

CLIMATE RESEARCH
Clim Res

Published online February 5

# Evaluation of climate patterns in a regional climate model over Italy using long-term records from SYNOP weather stations and cluster analysis

**S. Calmanti[1,*], A. Dell'Aquila[1], F. Maimone[2], V. Pelino[2]**

[1]Italian National Agency for New Technologies, Energy and Sustainable Economic Development (ENEA), CR Casaccia, Via Anguillarese 301, 00123 Santa Maria di Galeria, Rome, Italy

[2]Italian Air Force Centre for Weather and Climatology (CNMCA), Via Pratica di Mare, 00040 Pratica di Mare, Rome, Italy

ABSTRACT: We compare the output of a high-resolution regional climate model (RCM) with 40 yr of weather data from 64 weather stations from the Italian National Air Force network. Climatic zones were identified using the Ward's method for cluster analysis for minimum and maximum temperature and rainfall. The model is able to generate realistic spatial patterns of the observed clusters, although with different skills depending on the considered variable. The closest match between model and observations is for daily minimum temperature. The maximum temperature shows an unrealistic summer peak for most of the clusters. The model also consistently produces too many strong warm events during summer, and shows a tendency to overestimate total rainfall, especially during spring and early summer. The frequency and intensity of extreme events are well captured only for minimum temperature for Alpine and mountain weather stations. In spite of these biases and mismatches, this study shows, by means of a direct comparison with weather station data, that even in an area of complex orography and land–sea contrast such as the Mediterranean area, RCMs are able to produce realistic climate patterns at spatial scales that the global driver cannot capture.

KEY WORDS: Downscaling · Regional climate model · Climate model validation



## 1. INTRODUCTION

Climate impact studies require the downscaling and calibration of the output of General Circulation Models (GCMs) when climate information is needed at the local scale (Christensen et al. 2007, Fowler et al. 2007, Fowler & Wilby 2010, Teutschbein & Seibert 2010, Langner et al. 2012, Laprise et al. 2012, Tramblay et al. 2013) and when the focus is on the occurrence of extreme events (Beniston et al. 2007, Haarsma et al. 2013, Rajczak et al. 2013). A combination of Regional Climate Models (RCMs) and statistical methods is often adopted for these purposes. In fact, in the processing chain that converts the global scale, coarse resolution climate projections into local scale information, the combination of dynamical (i.e. using RCMs) and statistical downscaling is often found to improve the quality of the climate information (Paeth & Diederich 2010, Guyennon et al. 2013, White & Toumi 2013).

A particular challenge is that a stationary relation between large scale (>1000 km) atmospheric circulation regimes and small scale (<100 km) climate patterns cannot be assumed, especially in the context of long-term (>30 yr) climate change studies. However, the studies of Dell'Aquila et al. (2012) and Carillo et al. (2012) have shown how RCMs may be able to correctly reconstruct sub-regional patterns (patterns with scale $L$ such that 100 km < $L$ < 1000 km) of ocean temperature and sea level which are not described in

*Corresponding author: sandro.calmanti@enea.it

the corresponding global drivers. Other aspects of the added value provided by RCMs over the Mediterranean area include surface temperature (Feser 2006), rainfall (Im et al. 2010, Rauscher et al. 2010, Önol 2012) and sea surface wind in the proximity of complex topograpy (Artale et al. 2010, Herrmann et al. 2011, Winterfeldt et al. 2011), as well as other more complex environmental parameters (Carillo et al. 2012, Dell'Aquila et al. 2012)

In this study we assess the ability of a RCM—the PROTHEUS system described by Artale et al. (2010)—to produce intermediate scale patterns of atmospheric variability over the Italian peninsula. This area, with its complex orography and coastlines, is a particularly interesting case for testing the ability of RCMs to reproduce sub-regional climate patterns for use as an input for impact studies. At the typical resolution of state-of-the-art RCMs adopted for impact studies (20 to 50 km), the model output is not directly comparable with the spatial scale of information obtained from weather stations (e.g. D'Onofrio et al. 2014). Here, instead of disaggregating the climate model output to generate information that is directly comparable with weather station data, we aggregate both weather station and climate model data to identify a common spatial pattern, and thus enabling a comparison of the two kinds of data.

We identify sub-regional climatic patterns using the Ward's method for cluster analysis, which has proved to yield useful insights in the analysis of climate data and weather typing (Gong & Richman 1995, Unal et al. 2003, Wilks 2011, Vrac et al. 2007, Pinto et al. 2013). The reference observational sub-regional patterns are derived from daily records of minimum and maximum temperature and precipitation ($T_{max}$, $T_{min}$, P) from 64 weather stations maintained by the Italian Air Force Centre for Weather and Climatology (CNMCA). The weather stations and the corresponding model grids are grouped into different climate types by considering similarities in the seasonal cycle of $T_{max}$, $T_{min}$, and P. For each cluster we also analyse the model's ability to capture large deviations from the corresponding reference seasonal cycle, which is typically of interest for impact studies.

The aim of this work is to help identify the weaknesses in different areas of the model domain and potentially associated with a poor description of local processes, such as energy fluxes at the interface between the atmosphere and the Earth's surface or sub-grid atmospheric processes (convection). We also aim to provide a useful benchmark for the improvement of the RCM adopted for this study.

## 2. MODEL AND DATA

### 2.1. Observations

The observational dataset consists of daily temperature and precipitation records from 64 weather stations of the Italian Air Force network[1] from 1 January 1958 to 31 December 1999. These data, quality controlled according to the WMO standards (WMO 1983), are encoded with the meteorological messaging system (SYREP) which contains daily reports of temperature (minimum and maximum), twice daily cumulated rainfall, and wind speed and direction. In this study we focus on temperature and rainfall only, and the 64 weather stations have been chosen from a larger dataset to optimize time coverage and continuity during the considered period. Missing data are limited (<5%), and allow for a robust reconstruction of the seasonal cycle and an accurate evaluation of the corresponding large deviations. The names and locations of the 64 weather stations considered for this analysis are listed in Table 1. The weather stations are distributed fairly uniformly over the Italian peninsula (Fig. 1), except for an area of missing weather stations in central Italy, on the eastern flank of the Apennines and along the coast of the Adriatic Sea. Three of the weather stations are located on small islands (Ponza, Ustica and Pantelleria) and the elevations of the weather stations range from coastal, just above the sea level, to >2000 m a.s.l., and from 37.82° to 46.89° N, thereby covering a wide range of different climatic conditions.

### 2.2. Model

The Regional Earth System Model ENEA-PROTHEUS is described in Artale et al. (2010). It is a coupled, ocean-atmosphere limited-area model whose atmospheric component has a uniform horizontal grid spacing of 30 km on a Lambert conformal projection and 18 σ-levels. The simulation is performed on an area ranging from 20° to 60° N, which covers the entire Mediterranean Sea with lateral boundary conditions provided every 6 h by interpolating horizontal wind components, temperature, specific humidity and surface pressure from ERA-40 for the period 1958–2000 (Uppala et al. 2005). Sea surface temperature (SST) over the Atlantic is taken

[1]Information on the availability of weather data can be found at the URL: http://clima.meteoam.it/informazioni_en.php?type=generalita

Table 1. Name, international code (ID), coordinates and elevation (m) of weather stations from which observed data was obtained. Numbers in the left hand columns refer to the locations shown on the map in Fig. 1

| No. | Name | ID | Long. °E | Lat. °N | Elevation | No. | Name | ID | Long. °E | Lat. °N | Elevation |
|---|---|---|---|---|---|---|---|---|---|---|---|
| **1** | S. Valentino alla Muta | 8 | 10.50 | 46.83 | 1461 | **33** | Termoli | 232 | 15.05 | 42.01 | 44 |
| **2** | Passo Rolle | 21 | 11.78 | 46.30 | 2006 | **34** | Guidonia | 234 | 12.73 | 42.02 | 89 |
| **3** | Paganella | 22 | 11.03 | 46.15 | 2129 | **35** | Roma Ciampino | 239 | 12.58 | 41.78 | 105 |
| **4** | Dobbiaco | 33 | 12.20 | 46.70 | 1226 | **36** | Latina | 243 | 12.90 | 41.55 | 26 |
| **5** | Tarvisio | 40 | 13.55 | 46.50 | 778 | **37** | Frosinone | 244 | 13.30 | 41.63 | 185 |
| **6** | Rivolto | 45 | 13.02 | 45.95 | 52 | **38** | Pratica di mare | 245 | 12.45 | 41.65 | 21 |
| **7** | Torino Caselle | 59 | 7.65 | 45.22 | 301 | **39** | Campobasso | 252 | 14.65 | 41.57 | 807 |
| **8** | Torino Brik della Croce | 61 | 7.73 | 45.03 | 710 | **40** | Grazzanise | 253 | 14.07 | 41.05 | 10 |
| **9** | Cameri | 64 | 8.67 | 45.52 | 169 | **41** | Monte S.Angelo | 258 | 15.95 | 41.70 | 847 |
| **10** | Milano Linate | 80 | 9.27 | 45.42 | 107 | **42** | Amendola | 261 | 15.72 | 41.53 | 60 |
| **11** | Piacenza | 84 | 9.73 | 44.92 | 138 | **43** | Trevico | 263 | 15.23 | 41.05 | 1093 |
| **12** | Ghedi | 88 | 10.28 | 45.42 | 97 | **44** | Ponza | 280 | 12.95 | 40.92 | 185 |
| **13** | Villafranca | 90 | 10.87 | 45.38 | 68 | **45** | Potenza | 300 | 15.8 | 40.63 | 845 |
| **14** | Istrana | 98 | 12.10 | 45.68 | 42 | **46** | Capo Palinuro | 310 | 15.28 | 40.02 | 185 |
| **15** | Treviso S. Angelo | 99 | 12.18 | 45.65 | 23 | **47** | Gioia del Colle | 312 | 16.93 | 40.77 | 352 |
| **16** | Venezia Tessera | 105 | 12.33 | 45.50 | 2 | **48** | Latronico | 316 | 16.02 | 40.08 | 896 |
| **17** | Trieste | 110 | 13.75 | 45.65 | 35 | **49** | Brindisi (Casale) | 320 | 17.95 | 40.65 | 10 |
| **18** | Passo della Cisa | 124 | 9.93 | 44.43 | 1039 | **50** | Lecce | 332 | 18.15 | 40.23 | 53 |
| **19** | Luni Sarzana | 125 | 9.98 | 44.08 | 10 | **51** | Capo Bonifati | 337 | 15.88 | 39.58 | 485 |
| **20** | Monte Cimone | 134 | 10.70 | 44.20 | 2173 | **52** | Monte Scuro | 344 | 16.4 | 39.33 | 1677 |
| **21** | Bologna B. Panigale | 140 | 11.30 | 44.53 | 36 | **53** | S. Maria di Leuca | 360 | 18.35 | 39.82 | 112 |
| **22** | Marina di Ravenna | 146 | 12.30 | 44.45 | 6 | **54** | Ustica | 400 | 13.18 | 38.70 | 243 |
| **23** | Rimini | 149 | 12.62 | 44.03 | 13 | **55** | Messina | 420 | 15.55 | 38.20 | 54 |
| **24** | Capo Mele | 153 | 8.17 | 43.95 | 221 | **56** | Trapani Birgi | 429 | 12.50 | 37.92 | 9 |
| **25** | Pisa | 158 | 10.38 | 43.68 | 7 | **57** | Prizzi | 434 | 13.42 | 37.72 | 1035 |
| **26** | Monte Argentario | 168 | 11.17 | 42.38 | 631 | **58** | Gela | 453 | 14.22 | 37.08 | 33 |
| **27** | Firenze Peretola | 170 | 11.20 | 43.80 | 40 | **59** | Catania Sigonella | 459 | 14.92 | 37.4 | 293 |
| **28** | Arezzo | 172 | 11.85 | 43.47 | 249 | **60** | Pantelleria | 470 | 11.97 | 36.82 | 198 |
| **29** | Grosseto | 206 | 11.07 | 42.75 | 7 | **61** | Cozzo Spadaro | 480 | 15.13 | 36.68 | 51 |
| **30** | Viterbo | 216 | 12.05 | 42.43 | 308 | **62** | Decimomannu | 546 | 8.97 | 39.35 | 229 |
| **31** | Monte Terminillo | 219 | 12.98 | 42.47 | 1875 | **63** | Capo Bellavista | 550 | 9.72 | 39.93 | 150 |
| **32** | Vigna di valle | 224 | 12.22 | 42.08 | 266 | **64** | Cagliari Elmas | 560 | 9.07 | 39.25 | 2 |

from the Global Sea-ice and Sea Surface Temperature (GISST) dataset (Met Office Hadley Centre et al. 2006). Land–atmosphere energy, water, and momentum fluxes are modeled with the biosphere-atmosphere transfer scheme (BATS; Dickinson et al. 1993) that simulates vegetation and hydrology. BATS uses soil layer of 3 m depth, subdivided into a surface layer and a vegetation-dependent root zone. Nineteen land cover/vegetation types are characterized in BATS by bulk flux resistance parameters such as roughness length, stomatal resistance, leaf area index, surface and root zone soil depth, vegetation albedo and other aspects of the land–atmosphere interface.

The RCMl grid and the grid of the driving reanalysis are shown in Fig. 1. The time series at the weather station sites are extracted from the model output by averaging daily $T_{min}$, $T_{max}$ and P over a cell delimited by the 4 grid points nearest to each weather station. In the case of temperature, before computation of the cell average, the values at the model grid points are rescaled to weather station altitude by assuming a standard atmospheric lapse rate of 6.5 K $km^{-1}$ in the atmosphere, which is consistent with an approximately linear relation between the average temperature and the corresponding altitude of the considered weather stations (not shown). In the case of rainfall, a simple average of the 4 nearest grid points is considered. In the proximity of coastlines, one or more model grid points surrounding a given land based weather station may correspond to an ocean grid point. In those cases, only land grid points are considered for extracting model time series, in order to preserve the consistency of the climate regime described by the model with the local climate observed at the weather station site. No significant differences emerge in the cluster analysis described in the following section if the nearest neighbor or a simple bilinear interpolation are used to extract time series at the weather station site instead of using 4 grid points to calculate the cell averages.

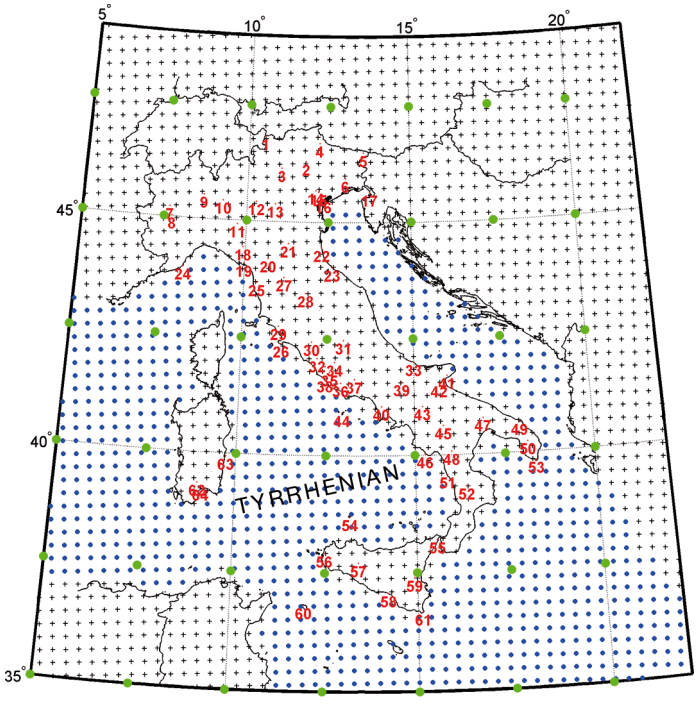


Fig. 1. Model grid over the focus area: land grid points (black crosses) and ocean grid points (blue dots). Red dots (sample points above numbers): weather stations; numbers correspond to those shown in Table 1, where the name, coordinates and elevation of each station is given. Green dots: grid of the driving reanalysis ERA40

## 3. CLUSTER ANALYSIS

### 3.1. Methods

The goal of cluster analysis is to detect objects (e.g. time series or spatial patterns) sharing some selected property, and to group them into homogeneous subsets. To this end, a definition of the similarity or distance between pairs of objects is necessary. Given $n$ objects, each composed of $p$ elements, organized in a data matrix $\boldsymbol{X}$ of dimension $n \times p$, one commonly used measure of the distance between 2 objects $i$ and $j$, which is also adopted here to define the distance between any 2 time series, is simply the Euclidean distance:

$$d_{ij} = \left[ \sum_{k=1}^{p} (x_{ki} - x_{kj})^2 \right]^{1/2} \quad (1)$$

Eq. (1) expands into an $n \times n$ distance (or proximity) matrix $\boldsymbol{D}$, which is symmetric with zero diagonal. In our case $n$ is the number of weather stations and $p$ is the length of the time series observed at each station. From the many clusterization algorithms we restricted ourselves to hierarchical agglomerative methods. Starting from the case of isolated single objects — each of the N weather stations identifies a cluster — the algorithm proceeds iteratively by joining cluster pairs with the smallest distance between them at each step. Different agglomerative methods can be constructed by adopting different definitions of the distance between the new clusters at each iteration. Say clusters A and B are joined at some step, because their separation distance $d_{AB}$ is the smallest. With the single-linkage method, the distance between the new cluster AB and another cluster C (i.e. the distance $d_{AB-C}$) is taken to be the smallest of the 2 distances between the original cluster and cluster C (i.e. $d_{AC}$ and $d_{BC}$). If the largest distance is chosen, the method is called complete linkage, whereas by taking the average, then the method would be a simple average linkage.

One major drawback of these methods is that they do not take into account the number of members in clusters A and B, so that a cluster with relatively few members can influence the distance between the merged groups and the other clusters. To correct this inconvenience the distance is weighted with the size of the clusters as follows:

$$d_{AB-C} = (N_A d_{AC} + N_B d_{BC}) / (N_A + N_B) \quad (2)$$

The resulting method is known as group average linkage, or simply the Ward method (Ward 1963) and is adopted in this study by applying it to the standardized time series of monthly data. Furthermore, in the Ward method, the merging of N + 1 clusters into N clusters is done by using a least-squares criterion to minimize the internal variability of all the clusters.

A useful graphical representation of the clustering structure of a set of objects is the dendrogram, which consists of many U-shaped lines connecting objects in a hierarchical tree. The height of each U represents the distance between 2 objects being connected and each 'leaf' in the dendrogram represents 1 data object. A critical aspect in many practical applications of cluster analysis is the selection of a significant number of clusters into which the initial dataset should be split. Although some degree of subjectivity is often unavoidable, a certain level of clustering may be more appropriate than others. The method adopted in this work is to monitor the distance between the clusters merged at each step and to set the cut-off to correspond with the transition from a 'plateau' (i.e. a situation where the distance between merged clusters remains relatively constant) to a sudden increase in the distances between merged clusters. We hereafter refer to the cut-off level as to the number of clusters identified by setting the cut-off at a given distance. Lower (higher) cut-off levels correspond to a lower (higher) number of clusters. For example, in Fig. 2a a Level 4 cutoff corre-

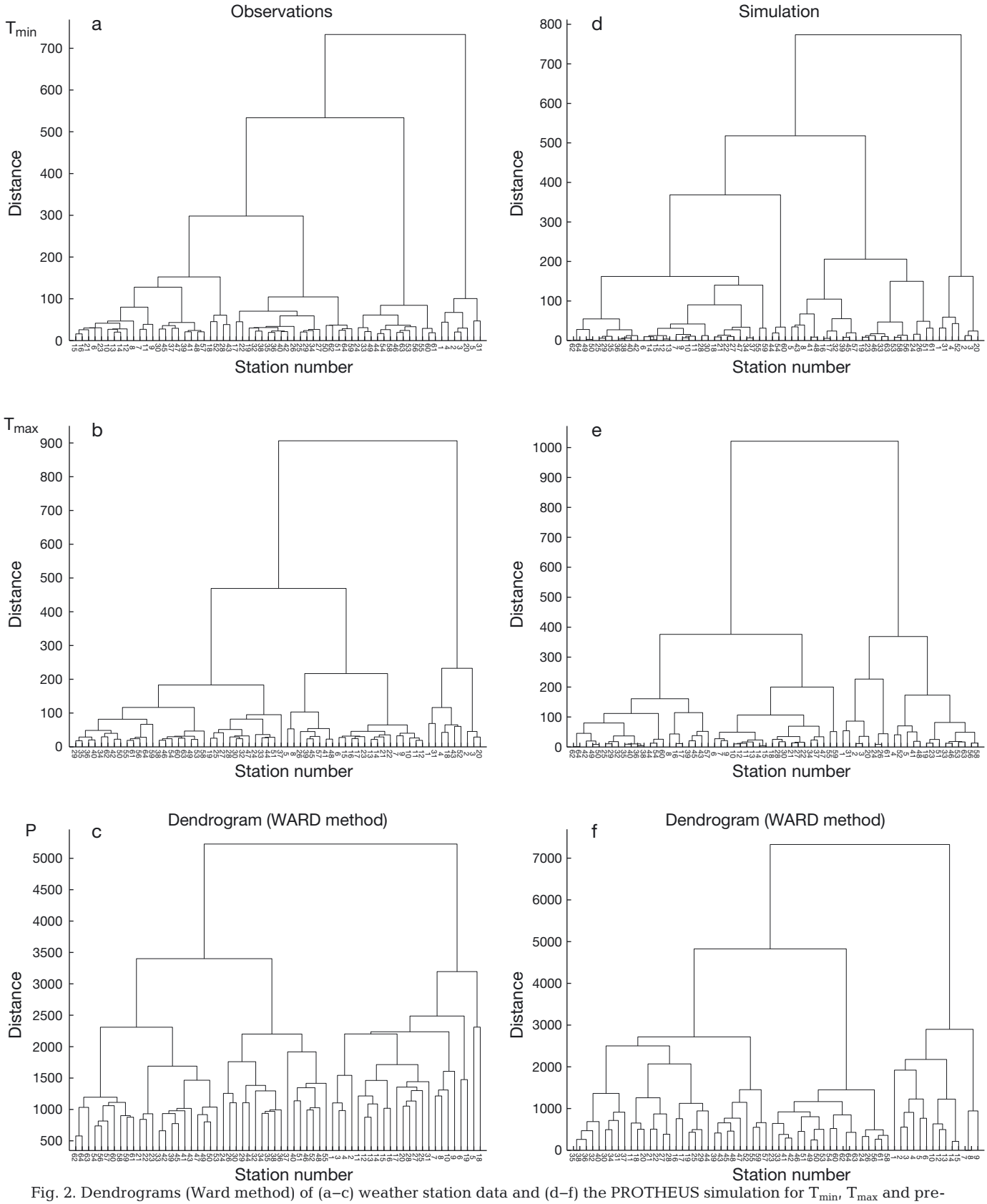


Fig. 2. Dendrograms (Ward method) of (a–c) weather station data and (d–f) the PROTHEUS simulation for $T_{min}$, $T_{max}$ and precipitation (P). Dendrograms are computed by using standardized variables; therefore, the distance between clusters has no unit

sponds to choosing the cut-off distance at a value of 250, whereas a lower cut-off level, i.e. Level 3, corresponds to a cut-off distance of about 400.

### 3.2. Results

Table 2 is a 'coincidence table' showing the degree of correspondence between observed and modeled clusters for $T_{max}$, $T_{min}$ and P. The number of clusters in each case was determined by the choice of cut-off level, which is further discussed below. Although the naming of clusters is arbitrary, the correspondence between observed and modeled clusters is established by considering their geographical overlap, except for the case of $T_{max}$ which is more problematic and is discussed in more detailed in Section 3.2. In the coincidence table, the main diagonal shows the number of sites associated to the same cluster both in the model and based on the analysis of observed values. The off-diagonal elements of the table correspond to sites associated to different clusters. Table 2 shows that the best agreement between model and observations is obtained for $T_{min}$ (41 matching sites among the 64 weather stations, corresponding to 64% agreement). P has a similar amount of agreement (60%), whereas for $T_{max}$ the model has a significantly lower skill in capturing the observed clusters.

In the following sections we discuss the comparison between observed and modeled clusters in more detail.

Table 2. Coincidence table for $T_{min}$, $T_{max}$ and P. Each cell in the table shows the number of sites associated to the observed cluster (Obs) and modeled cluster (Mod) indicated in the corresponding row and column headers. Diagonal cells in **bold**: number of matching sites assigned to the same cluster. Parentheses: percentage of total matches for each variable

| | Mod 1 | Mod 2 | Mod 3 | Mod 4 |
|---|---|---|---|---|
| **$T_{min}$ (64%)** | | | | |
| Obs 1 | **6** | 6 | 1 | |
| Obs 2 | 14 | **30** | 0 | |
| Obs 3 | 1 | 1 | **5** | |
| **$T_{max}$ (28%)** | | | | |
| Obs 1 | **13** | 8 | 11 | 2 |
| Obs 2 | 4 | **12** | 3 | 2 |
| Obs 3 | 1 | 1 | **2** | 5 |
| Obs 4 | 0 | 0 | 0 | 0 |
| **P (60%)** | | | | |
| Obs 1 | **15** | 13 | 0 | |
| Obs 2 | 0 | **9** | 4 | |
| Obs 3 | 0 | 8 | **15** | |

#### 3.2.1. $T_{min}$

For $T_{min}$, in the case of observed data from weather stations (Fig. 2a), a cut-off level corresponding to 3 or 4 clusters would be the obvious choice since the distance between the corresponding groups shows a steep increase at these levels. In particular the choice of a Level 4 cut-off would be justified by the clear separation from other higher clusterization levels. However, in the case of the model weather stations clusters (Fig. 2d), a more obvious choice would be a Level 3 cut-off, while cut-offs at higher levels would be more difficult to justify in terms of the relative increase in the corresponding distance between groups. Therefore, in the case of $T_{min}$, a cut-off level of 3 clusters was selected for comparing the model to observed data.

With regard to observed data, one cluster is composed mainly of coastal weather stations (Cluster 1, Fig. 3a) on both sides of the Italian peninsula.

A second cluster (Cluster 2, Fig. 3a) includes inland weather stations in the Po Valley, as well as weather stations mostly located away from the coast at intermediate elevations above sea level. Note that by setting the cut-off level to 4, this large group of weather stations would split into 2 different groups, one composed of weather stations at intermediate elevations along the Apennines, and the other composed of weather stations in the Po Valley and on the western flank of the Apennines. However, a Level 3 cut-off proves to be the optimal choice for a comparison with this particular model simulation, as it is discussed later on this section.

The third cluster consists of weather stations located in mountain areas (Cluster 3, Fig. 3a), at elevations ranging from 778 m (Stn 4, Dobbiaco) to 2173 m (Stn 20, Monte Cimone). This cluster includes weather stations over the Alps and over the Appennines, including southern Italy.

The clustering of the model output shows a structure which is very similar to the observations (Fig. 3a,d) if a Level 3 cut-off is selected. The cluster of coastal weather stations (Cluster 1) is reasonably well captured, although a few weather stations along the Apennines in southern Italy are erroneously attributed to this cluster. The cluster of mountain weather stations (Cluster 3) is also well resolved with the exception of 2 weather stations, one in the eastern Alps (Stn 5, Tarvisio), which is attributed to Cluster 1 in the model, and one in southern Italy (Stn 52, Monte Scuro), which is not attributed to Cluster 3 in the data from weather stations. The majority of the model grid is attributed to a single cluster (Cluster 2),

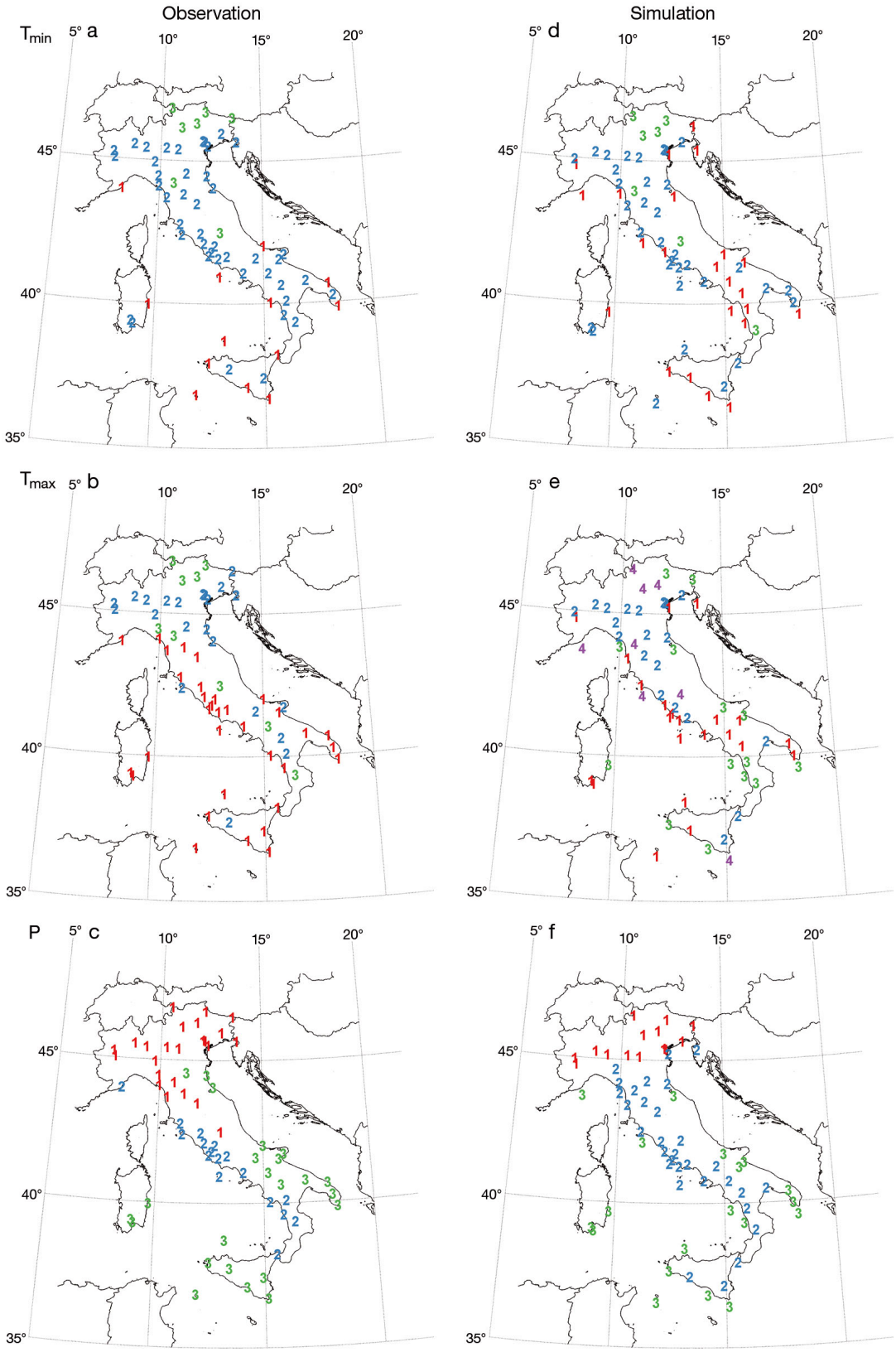


Fig. 3. Spatial clusters for (a–c) weather station data and (d–f) the PROTHEUS simulation for $T_{min}$, $T_{max}$, and precipitation (P). The numbering of clusters is arbitrary. Colors used only to emphasize the geographical structure of the clusters

which includes grid points all along the peninsula. However, if the number of clusters were increased, it would not be possible to establish a close relation between the weather station clustering and the model data clusters. Therefore a Level 3 cut-off was adopted for the variable $T_{min}$ as the maximum level of clusterization practicable for climate model under review.

### 3.2.2. $T_{max}$

The dendrogram for $T_{max}$ for the weather stations suggests a well-defined cut-off at Level-3 (Fig. 2b), whereas a possible higher cut-off would correspond to 6 clusters, since the distances corresponding to 4, 5 and 6 clusters are all bundled in a relatively narrow range. By choosing a Level 3 cut-off for the weather stations, a cluster of mountain weather stations is captured (Cluster 3, Fig. 3b), very similar to the case of minimum temperature. However, in contrast to $T_{min}$, a second cluster is composed mainly of the weather stations located along the Po Valley in northern Italy and a few others along the peninsula (Cluster 2). The cluster of coastal weather stations (Cluster 1) is larger than for $T_{min}$ and includes most of the weather stations along the Tyrrhenian Sea. A refinement of the clusterization (not shown) would split each of the 3 clusters above in 2, thereby producing 6 clusters. The coastal weather stations (Cluster 1) would divide into 2 sub-groups, one to the north and one to the south of the peninsula; Cluster 2 would split into one cluster located over the smaller Po Valley, and a second cluster along the Apennines; Cluster 3 would also split into 2 sub-groups, characterized by the altitude of weather stations.

The dendrogram of model grid points (Fig. 2e) is of a rather different structure than in the case of weather stations, thereby highlighting the potential for significant mismatches in the geographical structure of climatic clusters. For the model grid points, a Level 2 cut-off would be a natural choice for the clustering, since it corresponds to a steep increase in the distance among the corresponding groups with respect to higher cut-offs. On the other hand, a Level 4 cut-off would produce clusters with a geographical pattern that is very different from observations (Fig. 3b,e).

Thus, in the case of $T_{max}$, it is difficult to identify a common cut-off level that is appropriate for both modeled and observed data. In particular, a further refinement of the clusterization, applying a higher cut-off level, would reduce the match between the observed and the modeled clusters.

Note that the cluster analysis of weather station data for $T_{max}$ and $T_{min}$ produces slightly different groupings of weather stations for the 2 variables. In general the $T_{min}$ clusters are better captured by the model. For $T_{max}$ the cluster of weather stations in the Po Valley (Cluster 2) is better characterized, whereas for $T_{min}$ the alpine cluster (Cluster 3) is more neatly composed of weather stations located above a certain altitude (see discussion above.)

### 3.2.3. Rainfall

In the case of rainfall a Level 4 cut-off for weather station data (Fig. 2c) seems to be a natural choice, as it corresponds to a steep increase in the relative distance between groups. However, one of the Level 4 clusters is composed of only 2 weather stations (Stn 5, Tarvisio and Stn 18, Passo della Cisa) and we decided, in order to simplify the analysis, to merge them into the group of the weather stations that are geographically closest. By contrast, in the case of model data (Fig. 2f), a Level 3 cut-off appears to be the most natural choice for a robust clustering, based on the criterion described in the discussion of the method in at the start of Section 3.

The spatial patterns of the identified clusters are relatively similar. For the weather station data, one group is composed of weather stations in northern Italy, including the Alps and the Po Valley, along with a few weather stations along the northern part of the Apennines (Cluster 1, Fig. 3c). The model produces a cluster with a similar pattern, except that it does not include the Apennines area. Another group of weather stations is located along the western Adriatic coast of Italy from north to south (Cluster 3). This cluster is also reproduced by the model, which however extends this cluster to the Apennines area.

Cluster 2 includes weather stations mainly in Tyrrhenian coastal areas and to the south of the peninsula. A similar cluster is detected in the model data although it is slightly less populated than for the observed data, with fewer sites in the southern Apennines.

To summarize, although the description of the observed climatic clusters produced by the PROTHEUS model is not extremely accurate, especially for the case of $T_{max}$, it represents a significant improvement on the accuracy that the coarse resolution global driver can achieve. As an example, the cluster of weather stations in the Eastern Alps (Stns 1, 2, 3 and 4) and a significant portion of the Po Valley cluster (Stns 12, 13, 14 and 15) are well separated both in

the observational dataset and in model data. By contrast, applying the coarse resolution global driver to derive local time series in the same way (by interpolation of the nearest land grid points) the Eastern Alps and the Po Valley clusters would not be identified. More importantly, all weather station sites would be undefined in southern Italy where the coarse resolution global driver does not have grid points over land.

## 4. VALIDATION OF CLUSTER CLIMATOLOGY

In this section we focus on the representation of the seasonal cycle of the inter-annual variability, and discuss the distribution of deviations from the seasonal cycle and the representation of intense events for each cluster and for each of the considered variables.

In order to examine the differences between the composition and geographical structure of the observed and the model clusters, as discussed in Section 3, we consider the observed clusters as a reference, and compute the average behavior of each cluster by averaging over the members of the observed cluster both for the weather station data and for the model data. The misalignment is considered to provide evidence of the systematic bias of the climate model.

### 4.1. Seasonal cycle

Figs. 4 & 5 and Fig. S1 in the Supplement at www.int-res.com/articles/suppl/c062p173_supp.pdf show the observed and modeled 5-d running mean ±1σ of seasonal cycles of $T_{min}$, $T_{max}$ and P respectively. Means were derived by averaging the mean climatological seasonal cycles of all weather stations in each cluster. Standard deviation was computed as the root mean square distance of the mean seasonal cycle of each weather station from the corresponding cluster average, thereby reflecting the spatial variability of the seasonal cycle within each cluster.

Fig. 4 shows the comparison between the modeled and the observed $T_{min}$ over the 3 observed clusters. The weather stations in the mountain cluster (Cluster 3 for $T_{min}$) are usually at high altitude and the seasonal cycle shows $T_{min}$ below freezing (<0°C) during winter, usually until the end of April, whereas the highest $T_{min}$ is ~10°C at the end of July and beginning of August. For this cluster, the model accurately reproduces the observed seasonal cycle although the variability within the cluster is over-estimated, due to the approximate altitude correction, in particular for the

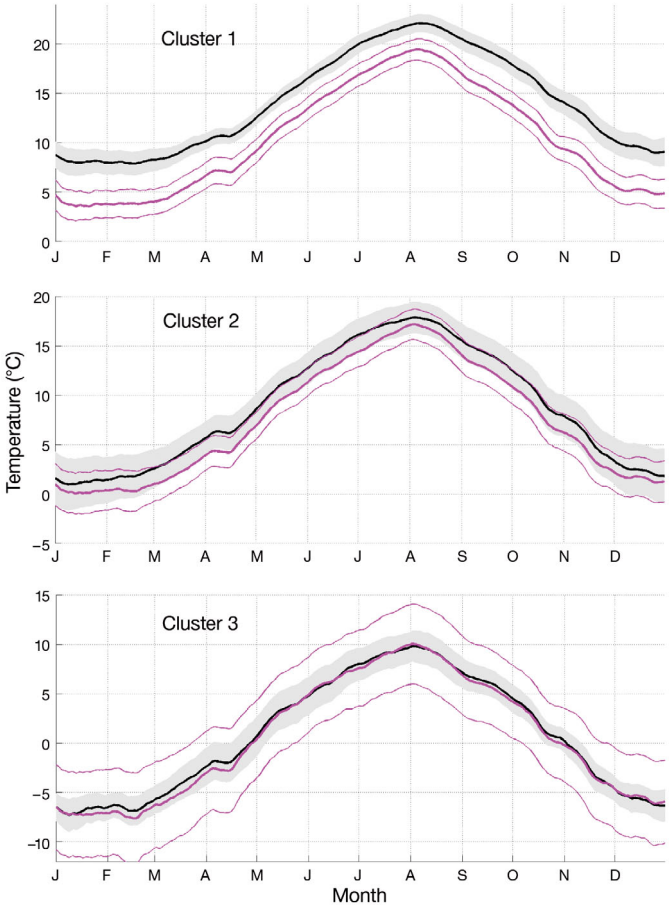


Fig. 4. Seasonal cycle of $T_{min}$ over the 3 observed clusters shown in Fig. 3a. Thick black lines: mean seasonal cycle for the weather station data. Grey shaded areas: range (±1σ) of spatial variability of weather station data within the cluster. Thick magenta lines: mean seasonal cycle (thin magenta lines: ±1σ) of the model output of the PROTHEUS simulation for the same clusters. To filter out the highest frequency noise we applied a 5 d running mean to the time series

weather stations in Cluster 3 (mountain weather stations): Stn 20, Monte Cimone (too warm after correction) and Stn 1, San Valentino (too cold after correction).

For Cluster 1, the model captures the amplitude and the temporal evolution of the seasonal cycle of $T_{min}$, although with a consistent negative bias. For Cluster 2, the model systematically underestimates $T_{min}$ but provides a good representation of the amplitude and temporal evolution of the seasonal cycle.

The model is less accurate in the description of the seasonal cycle of $T_{max}$, as shown in Fig. 5. The cluster of mountain weather stations (Cluster 3, Fig. 3b,e) shows the lowest $T_{max}$, with values that may fall below 0°C during winter. The largest amplitude of the seasonal cycle is in the Po Valley (Cluster 2), with relatively low $T_{max}$ during winter and summer $T_{max}$

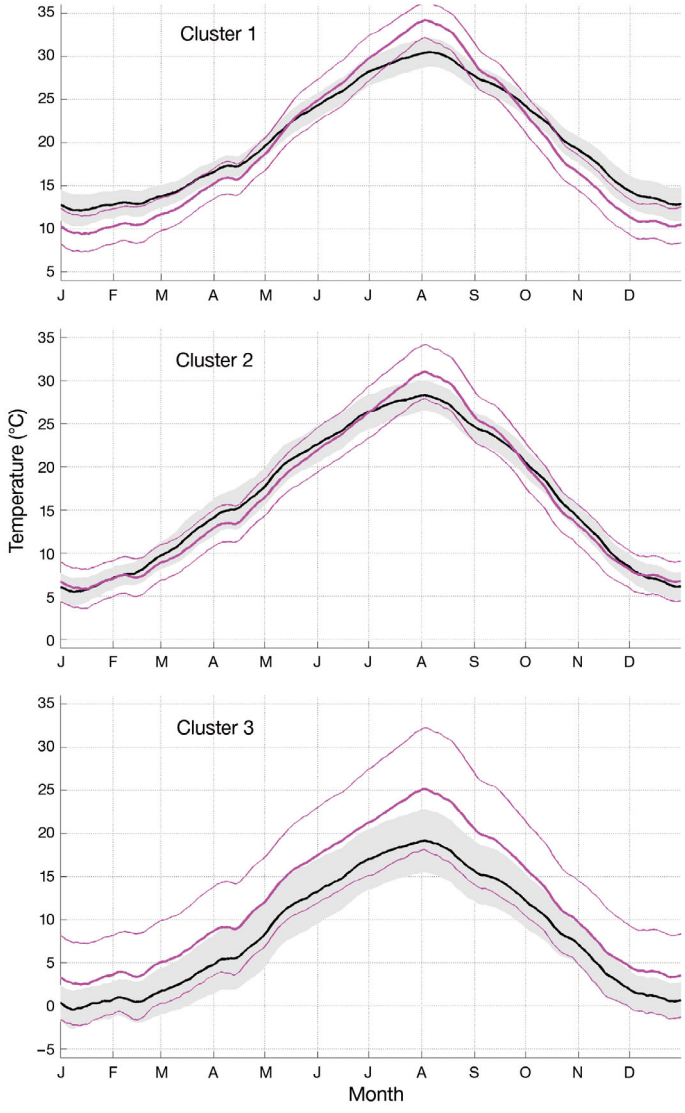


Fig. 5. Seasonal cycle of $T_{max}$ over the 3 observed clusters shown in Fig. 3b. For significance of lines and shading see the Fig. 4 legend

close to 30°C. Coastal weather stations (Cluster 1) have a weaker seasonal cycle: $T_{max}$ is usually >10°C even in winter, and reaches a maximum of ~30°C during summer. This cluster includes mainly weather stations in southern Italy and has a period of relatively stable, mild temperatures (~13°C) during winter.

For the coastal weather stations in Cluster 1, the most evident deficiency of the model is in capturing the amplitude of the seasonal cycle, with summer $T_{max}$ higher in the model than in observations, and with a peak of extremely high temperature at the beginning of August. A possible explanation for the misrepresentation of summer temperature is a poor description of the surface energy budget, related to land-cover characteristics and the parameterization of land-atmosphere energy fluxes (Anav et al. 2010). There is also a systematic underestimation of the winter temperature. The cool winter temperatures in coastal areas in the model are likely related to the cool bias in the PROTHEUS simulation of winter SST, already discussed by Artale et al. (2010). The closest match between observed and modeled $T_{max}$ is for the Po Valley weather stations (Cluster 2) where the model temperature is in agreement with observations over most of the year, except for the anomalous warming during summer.

In the case of rainfall, the seasonal cycle of observed clusters ranges from unimodal (1 single maximum during each solar year) to bimodal (2 maxima during the calendar year) as shown in Fig. S1. A marked unimodal behavior with a well-defined summer minimum is observed for the weather stations in central and southern Italy along the coast of the Tyrrhenian Sea and over the Apennines (Cluster 2, Fig. 3c) and for the weather stations in southern Italy and islands (Cluster 3, Fig. 3c). These 2 clusters differ in the amplitude of their seasonal cycles and of the corresponding spatial standard deviation. The smallest amplitude of the seasonal cycle is observed for Cluster 3. Although the model captures the summer minimum in the seasonal cycle of rainfall for Clusters 2 and 3, it tends to overestimates rainfall during spring. As a result, the model seasonal cycle of rainfall has a plateau between October and May, which is not seen in observations.

The weather stations in the Alpine area and in the Po Valley (Cluster 1, Fig. 3c) have a bimodal seasonal cycle with a weak minimum in August and in January–February. Similarly to Clusters 2 and 3, the model also overestimates the mean rainfall for this cluster and the associated standard deviation during the first part of the year. The relative maxima during May and October are associated with a large variability (shaded area), which corresponds to a higher probability of intense rainfall events (see Section 4.3). The bimodal seasonal cycle is well captured by the model, which however tends to have a late minimum in August–September, in contrast to the observed minimum in July–August.

### 4.2. Interannual variability

Regional climate models are expected to add value to the modeling of long-term impacts of climate variability and change. Therefore, it is important to assess how the observed variability and trend for the

different clusters are reproduced in the case of perfect boundary conditions, i.e. when the model is driven at the boundaries by the observed climate (the global reanalysis).

Figs. S2–4 in the Supplement compare, for each cluster, the observed and modeled long-term anomalies from the corresponding average season cycles following removal of the systematic biases discussed in Section 4.1. We define 'long-term anomaly' as the 5 d running mean of the daily anomalies of each quantity from the corresponding mean seasonal cycle. We compute the standard deviations (shaded areas in Figs. S2–4) by considering the anomalies of all weather stations within each cluster.

For $T_{min}$ (Fig. S2) the chronology of anomalies for the weather stations in the mountain area (Fig. S2c) is well reproduced but the model simulation tends to underestimate the warming trend after the 1980s. The spatial variability among the modeled weather stations for Cluster 3 is almost twice the spatial variability of the corresponding observations. In the other clusters, the overall spatial variability is well captured although, especially in the case of Cluster 2 (Po Valley and coastal weather stations), the model produces an intense warming event in 1989 (Fig. S2b) that is not evident in observations.

For $T_{max}$ (Fig. S3), the model performances are generally worse than for $T_{min}$. The long-term climate trend of $T_{max}$ reported in Fig. S3 is well captured only for mountain weather stations (Fig. S3c). For this cluster, modeled anomalies capture the warming trend between the 1980s and the 1990s and the warm event in 1989. For the other 2 clusters, the model shows an unrealistic period of negative anomalies during the 1970s, especially for the coastal weather stations (Fig. S3a). Simulations also show a rise in temperature during the 1980s, leading to a warm event in 1989 as in the case of mountain cluster; however, this event is not evident in observations for Clusters 1 and 2. An analysis of the simulation conducted using the same model by Artale et al. (2010) shows a similar mismatch of the modeled warm event in a comparison with the observed SST. In the model, the poor description of $T_{max}$ is likely related to an incorrect description of soil–atmosphere interaction, especially over central-southern Italy. This so-called 'summer drying problem' in the PROTHEUS simulation (Mariotti & Dell'Aquila 2012) likely contributes to a misrepresentation of the summer $T_{max}$ in our study.

Rainfall anomalies (Fig. S4) over North-Central Italy (Clusters 1 and 2, Fig. 3c) show a wet period in the second part of 1970s in observational data. The model tends to overestimate this rainy phase as a consequence of a poor representation of the moisture content in the global driver ERA-40, discussed by Mariotti & Dell'Aquila (2012). This feature is particularly evident for weather stations in mountain areas and in the Po Valley (Cluster 1, Fig. 3c).

For the weather stations along the Tyrrhenian and Adriatic coasts (Clusters 2 and 3, Fig. 3c) an observed negative trend in precipitation during the 1980s is also shown in the model, although with an excess drying towards the end of this decade. The spatial variability associated with each cluster is also well reproduced by the regional model.

### 4.3. Deviations from the seasonal cycle and intense events

In view of the potential use of the model output in impact studies focusing on extreme events such as heat and cold waves, or floods, it is important to evaluate the model performance in capturing the distribution of large deviations from the reference seasonal cycle and the frequency and seasonality of the largest anomalies.

Figs. 6–8 show the distribution of the deviations from seasonal mean values. For each cluster, the probability density functions (PDFs) of deviations are derived by considering all daily anomalies from the respective average seasonal cycles of all weather stations in the cluster (or model time series). We performed Kolmogorov-Smirnov (K-S) tests for the null hypothesis that 2 PDFs extracted from observations and from model output are equal at the 99% confidence level. Then, for each cluster and for each variable ($T_{min}$, $T_{max}$, P) we counted the number of events exceeding a selected threshold (i.e. $\pm 2\sigma$ of each weather station distribution) with the aim of validating the occurrence of large deviations regardless of existing model biases (Figs. 8–10). The $\sigma$ values were derived from the full distribution of daily anomalies, i.e. large deviations from the seasonal cycle were selected at thresholds that were independent of the specific season. In particular, we considered large positive anomalies of $T_{max}$ and P, but with large negative anomalies of $T_{min}$, i.e. anomalies that are directly connected to the occurrence of hazards such has heat waves, floods and freezing days.

For $T_{min}$ the distribution of anomalies for weather stations and for the model data are statistically equivalent only for the case of the weather stations in mountain areas, i.e. Cluster 3 (Fig. 6). The seasonality of cold events (Fig. 9e) for Cluster 3 is also well reproduced in the model. The events were counted

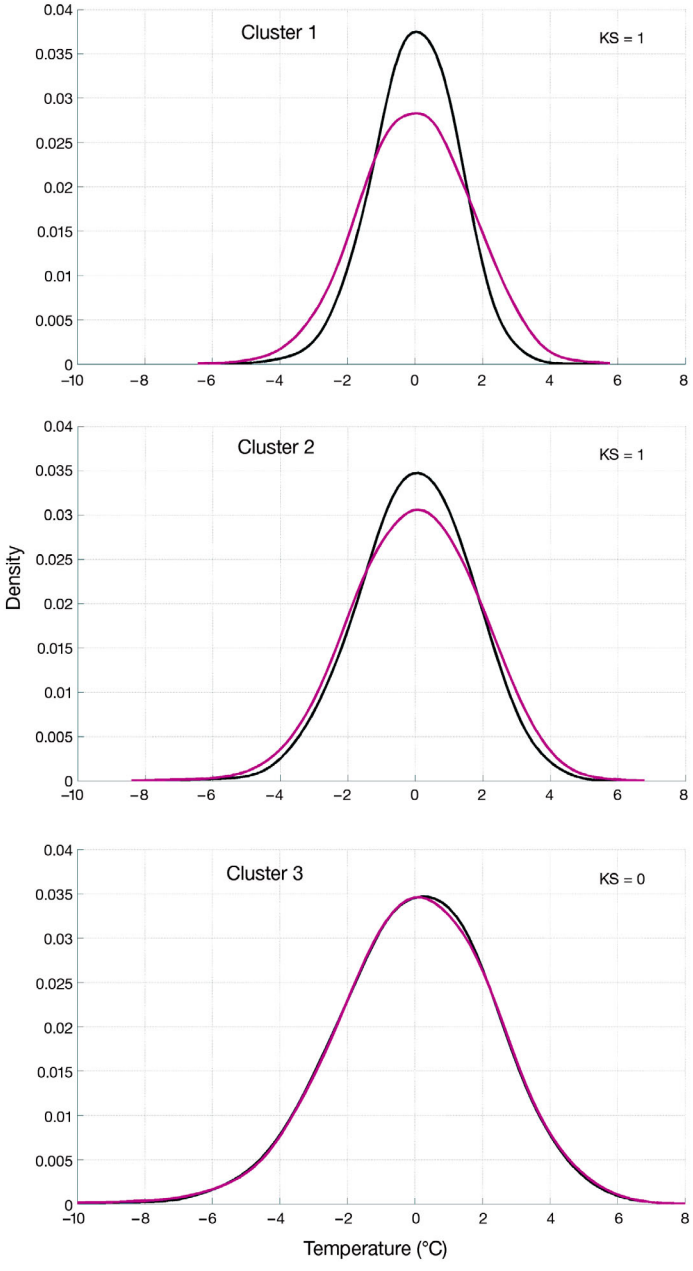


Fig. 6. Probability density functions of deviations from the seasonal cycle for $T_{min}$ (see Fig. S2 in the Supplement) for the 3 observed clusters shown in Fig. 3a. Black thick lines: mean values of the weather station data. Thick magenta lines: mean values for model output of the PROTHEUS simulation. PDFs are smoothed using a kernel function estimator and by adopting a width parameter $h = 3.5 \times \Delta$, where $\Delta$ is the bin amplitude. We assume 100 bins in the interval between the minimum and maximum length

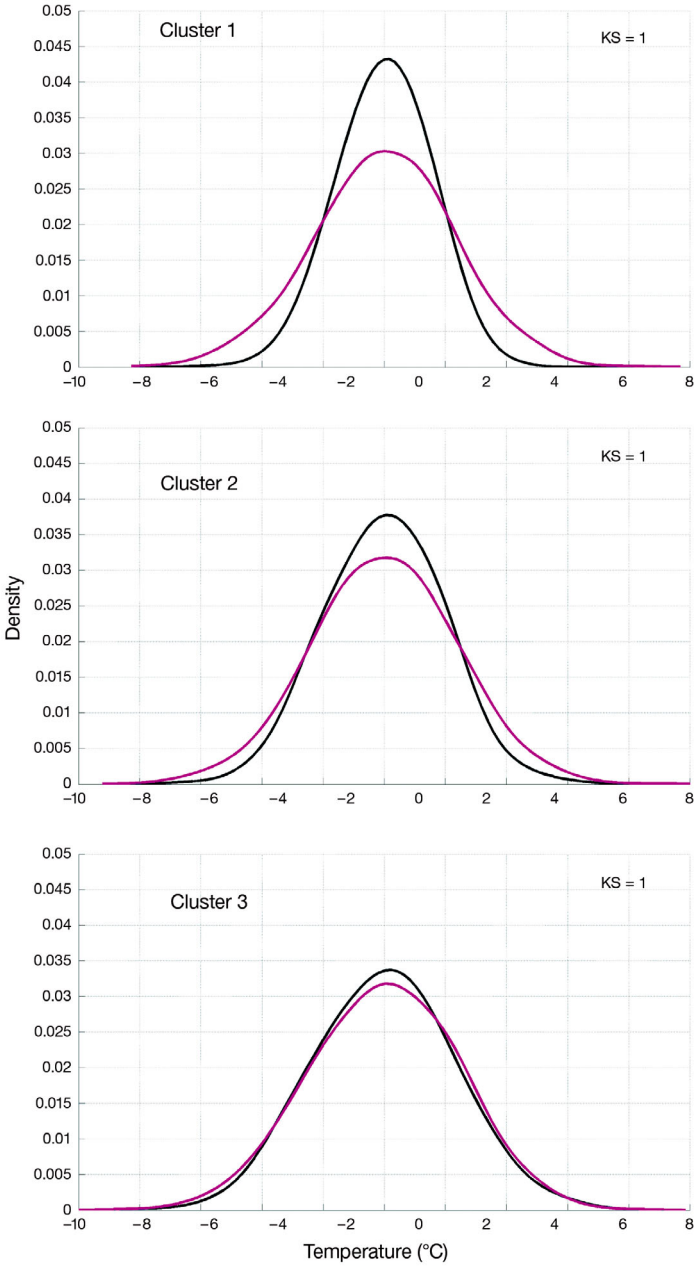


Fig. 7. PDF anomalies of the deviations from seasonal cycle for $T_{max}$ (see Fig. S3 in the Supplement) for the 3 observed clusters shown in Fig. 3b. For significance of lines and details of the method see the Fig. 6 legend

by considering the daily values that exceeded the selected threshold. As a reference, a hundred events correspond to roughly 0.03% of the entire sample of daily anomalies. In the case of $T_{min,}$ for the weather stations along the Apennines and in the Po Valley (Cluster 2, Fig. 3a), the distribution of anomalies shows thicker tails for the model, which reflects an overall overestimation of cold events, especially during spring. A similar behavior, with thicker extreme tails, is obtained for $T_{min}$ in the case of Cluster 1, where there are systematically too many cold events compared with the observed data.

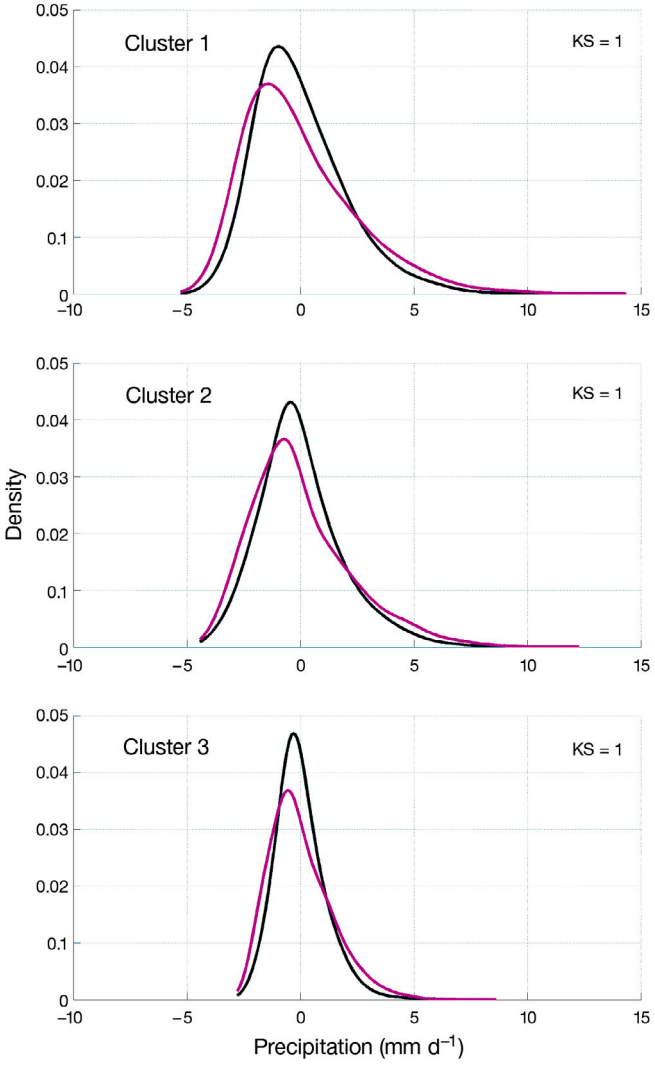


Fig. 8. PDF anomalies of the deviations from seasonal cycle for precipitation (P) (see Fig. S4 in the Supplement) for the 3 observed clusters shown in Fig. 3c. For significance of lines and details of the method see the Fig. 6 legend

For $T_{max}$, the model performances for all clusters are generally poorer than for $T_{min}$, and the K-S test shows that the distribution of modeled deviations are always statistically different from observed deviations. In particular, for the Clusters 1 and 2, the tails of the distributions are more populated in the PROTHEUS simulation than in the weather station data. Furthermore, warm events show a rather different seasonality depending on the cluster (Fig. 9b,d). For the weather stations in mountain area (Cluster 3, Fig. 3b), warm anomalies are observed especially during spring (MAM, Fig. 9f), whereas the model shows a rather uniform occurrence of warm anomalies throughout the year, with only a weak tendency for more warm anomalies during summer. In the Po Valley (Cluster 2, Fig. 3b), most observed strong warm anomalies occur during MAM, while for the coastal weather station (Cluster 1, Fig. 3b), warm anomalies occur especially during JJA. By contrast, in the model, warm events occur during JJA for both Clusters 1 and 2, thereby confirming that underestimation of soil moisture during summer can easily lead to overestimating the occurrence of warm events. This overestimation is enhanced by positive feedback between soil moisture and temperature, with higher surface temperature leading to drier soils and less evapotranspiration, thus further increasing surface temperatures.

The distribution of rainfall anomalies resembles, as expected, a gamma distribution (Fig. 8). The observed and the modeled distributions are significantly different for all clusters according to K-S test at the 95% significance level. In particular, the tails for intense rainy events are more populated in the model simulation. This is confirmed in Fig. 10, which shows the seasonality of intense precipitation events. According to the weather station data, SON is the principal period for intense precipitation events over Italy. In particular, rainy events occur during SON when deep cyclogenesis events in the lee of the Alps lead to strong precipitation over Northern and Central Italy. The model is able to capture the occurrence of intense rainfall events during SON. However, the model systematically overestimates the frequency of intense precipitation during MAM and JJA.

## 5. CONCLUSIONS

This study compared the output of a high-resolution RCM with 40 yr of daily weather data from 64 weather stations maintained by the Italian National Air Force. The aim was to provide a benchmark for the evaluation of a climate model, the PROTHEUS system, based on the model RegCM3, whose performance is mostly comparable to that of the latest model, version RegCM4, described in Giorgi et al. (2012).

We identified homogenous climatic zones using Ward's method for cluster analysis for $T_{min}$, $T_{max}$, and P. The observed climatology (seasonal cycle and interannual variability) and the distribution of the deviations from the climatology were compared to the corresponding model data. We constructed the model analogues of weather stations by considering the daily values for the model grids nearest to each weather station site. The aim was to evaluate the

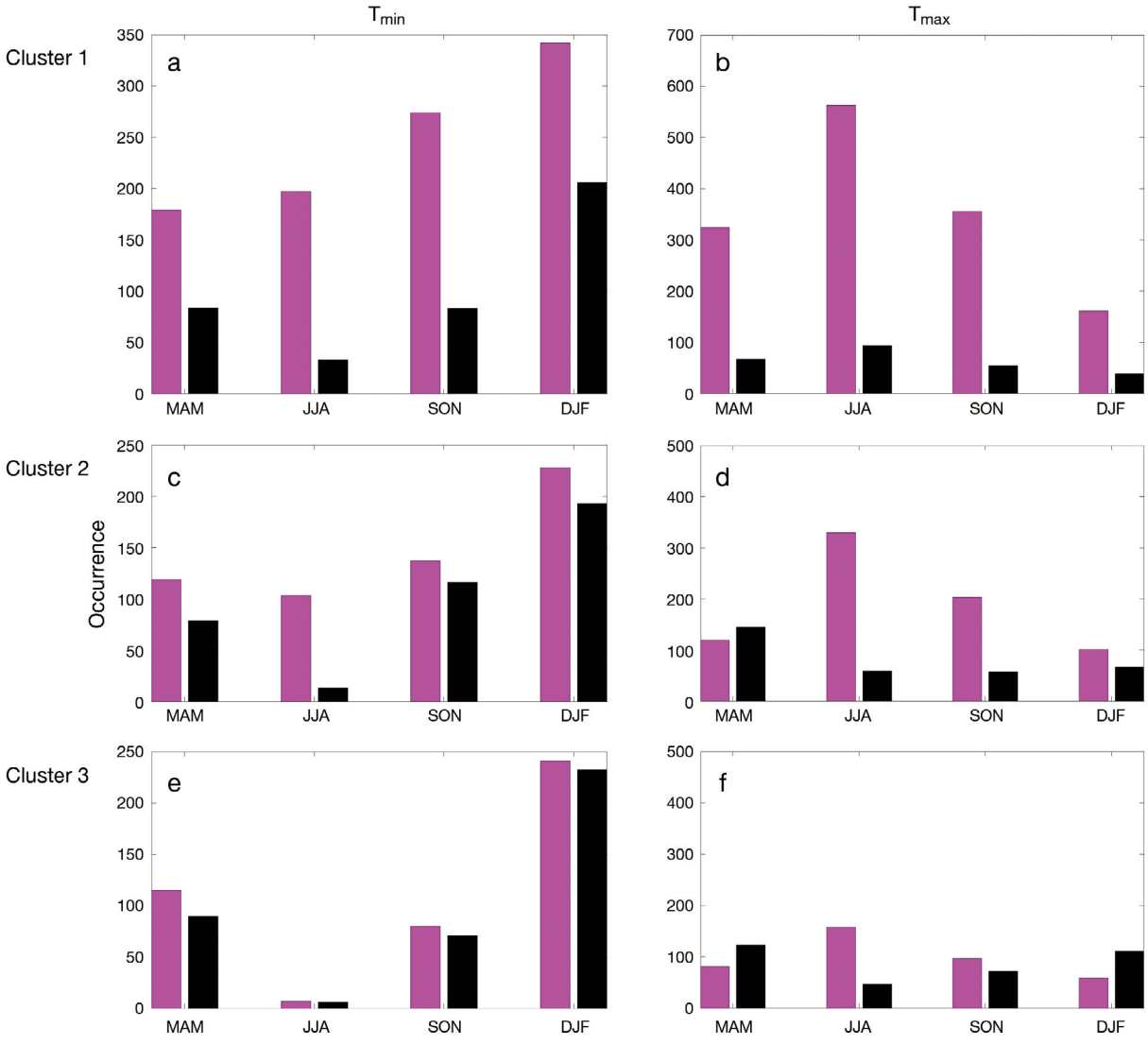


Fig. 9. Occurrence (number) of large (a,c,e) negative anomalies of $T_{min}$ and (b,d,f) positive anomalies of $T_{max}$ from seasonal means for weather station data (black bars) and PROTHEUS simulation model output (magenta bars). For $T_{min}$ ($T_{max}$), large negative (positive) discrepancies, i.e. cold (warm) events, are defined as those with anomaly values exceeding a threshold set at −2 (+2) standard deviations from the observed mean seasonal cycle for each cluster. Note the difference in *y*-axis scales. MAM: March–May; JJA: June–August; SON: September–November; DJF: December–February

model performances independently from additional adjustments and corrections of existing biases. We applied a simple adjustment to a standard atmospheric lapse rate in order to account for the differences between the real orography and the smoothed orography adopted in the model.

We conducted our analysis by first identifying 3 climatic clusters for each of the 3 considered variables. The model is able to capture realistic spatial patterns of the observed clusters, although with different skills, depending on the considered variable. As discussed in Section 3, the clustering over 3 climatic regions emerges as the optimal scale of spatial aggregation at which the model is able to reproduce the observed clusters. The closest match between model and observations is for the case of daily $T_{min}$. Rainfall shows a significant mismatch between model and observations, especially in central Italy along the Apennines. We found significant mismatches in the case of $T_{max}$. In particular, $T_{max}$ shows an unrealistic summer peak during summer over most of the considered domain. The poor model performances for $T_{max}$ are seen during 1989, and generally in the overestimation of warm events during JJA, when drier than normal soil during summer can initiate a positive feedback process.

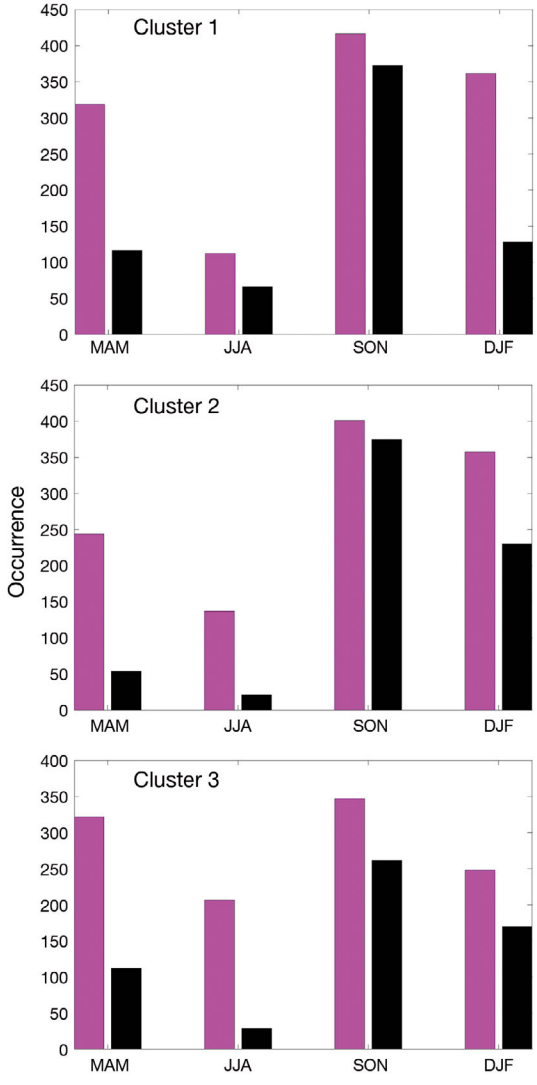


Fig. 10. Occurrence (number) of large positive anomalies of P from seasonal means for weather station data (black bars) and PROTHEUS simulation model output (magenta bars). Large positive discrepancies (rainfall events) are defined as those with anomaly values exceeding a threshold set at +2 standard deviations from the observed mean seasonal cycle for each cluster

The model also shows a tendency to overestimate total P, especially during spring and early summer. For the cluster of weather stations centered over northern Italy, the seasonal cycle is not well reproduced, whereas for the central and southern Italy, the model values are generally in closer agreement with observed rainfall patterns. A sizeable fraction of the total P during late spring and summer is linked to atmospheric deep convection (Claud et. al. 2012), and is therefore directly affected by locally available moisture and latent heat. Possible improvements to the model to reduce the late spring and summer mismatches could therefore be achieved by making adjustments to local land–atmosphere interactions through changes both in physiographic data and in the land–atmosphere energy fluxes and atmospheric deep convection. By contrast, during winter and fall, a large fraction of total rainfall is associated with well-characterized large scale circulation patterns (Toreti et al. 2010). In this case, a model improvement is likely to require substantial testing of the ability to correctly describe the propagation of synoptic scale circulation patterns.

We also analyzed, for each cluster and for each of the considered variables, the distribution of anomalies with respect to seasonal cycles, and the occurrence of intense events, defined as deviations from the corresponding seasonal cycle exceeding the threshold of 2 standard deviations. Reliable statistics of the distribution of the anomalies and of the frequency of intense events are produced only in the case of $T_{min}$ for Alpine and mountain weather stations, a result consistent with those from the cluster analysis and comparison of observed and modeled seasonal cycles.

Our analysis confirms, by means of a direct comparison with weather station data, that RCMs are able to produce realistic climate patterns at spatial scales that the global driver cannot capture, even in an area of complex orography and land–sea contrast such as the Mediterranean area. These results are consistent with the recent findings of D'Onofrio et al. (2014), who used the same RCM output analyzed in this study to demonstrate that the high-resolution precipitation fields obtained with a stochastic downscaling method are more similar to observations when the procedure is applied to the RCM output rather than to the global reanalyses. Therefore our work supports the conclusion that, with reliable coarse resolution global drivers available, RCMs can efficiently produce large ensembles of high resolution downscaling over dynamically complex target domains.

*Acknowledgements.* This work was supported by the DTA-MIUR NextData Project funded by the Italian Ministry for Education, University and Research.

LITERATURE CITED

Anav A, Ruti PM, Artale V, Valentini R (2010) Modelling the effects of land-cover changes on surface climate in the Mediterranean region. Clim Res 41:91–104

Artale V, Calmanti S, Carillo A, Dell'Aquila A and others(2010) An atmosphere-ocean regional climate model for the Mediterranean area: assessment of a present climate simulation. Clim Dyn 35:721–740

Beniston M, Stephenson DB, Christensen OB, Ferro CAT and others (2007) Future extreme events in European climate:

an exploration of regional climate model projections. Clim Change 81:71–95

Carillo A, Sannino G, Artale, V, Ruti PM, Calmanti S, Dell'Aquila A (2012) Steric sea level rise over the Mediterranean Sea: present climate and scenario simulations. Clim Dyn 39:2167–2184

Christensen JH, Carter TR, Rummukainen M, Amanatidis G (2007) Evaluating the performance and utility of regional climate models: the PRUDENCE project. Clim Change 81:1–6

Claud C, Alhammoud B, Funatsu BM, Lebeaupin-Brossier C, Chaboureau JP, Béranger K, Drobinski P (2012) A high resolution climatology of precipitation and deep convection over the Mediterranean region from operational satellite microwave data: development and application to the evaluation of model uncertainties. Nat Hazards Earth Syst Sci 12:785–798

D'Onofrio D, Palazzi E, von Hardenberg J, Provenzale A, Calmanti S (2014) Stochastic rainfall downscaling of climate models. J Hydrometeorol 15:830–843

Dell'Aquila A, Calmanti S, Ruti PM, Struglia MV, Pisacane G, Carillo A, Sannino G (2012) Impacts of seasonal cycle fluctuations in an A1B scenario over the Euro-Mediterranean. Clim Res 52:135–157

Dickinson RE, Kennedy PJ, Henderson-Sellers A (1993) Biosphere-atmosphere transfer scheme (BATS) version 1e as coupled to the NCAR community climate model. NCAR Technical Note NCAR/TN-387+STR, National Center for Atmospheric Research, Boulder, CO

Feser F (2006) Enhanced detectability of added value in limited-area model results separated into different spatial scales. Mon Weather Rev 134:2180–2190

Fowler HJ, Wilby RL (2010) Detecting changes in seasonal precipitation extremes using regional climate model projections: implications for managing fluvial flood risk. Water Resour Res 46:W03525, doi:10.1029/2008WR007636

Fowler HJ, Blenkinsop S, Tebaldi C (2007) Linking climate change modelling to impacts studies: recent advances in downscaling techniques for hydrological modelling. Int J Climatol 27:1547–1578

Giorgi F, Coppola E, Solmon F, Mariotti L, and others (2012) RegCM4: model description and preliminary tests over multiple CORDEX domains. Clim Res 52:7–29

Gong X, Richman MB (1995) On the application of cluster analysis to growing season precipitation data in North America east of the Rockies. J Clim 8:897–931

Guyennon N, Romano E, Portoghese I, Salerno F and others (2013) Comparing dynamical, stochastic and combined downscaling approaches—lessons from a case study in the Mediterranean region. Hydrol Earth Syst Sci 17:705–720

Haarsma RJ, Hazeleger W, Severijns C, de Vries H and others (2013) More hurricanes to hit western Europe due to global warming. Geophys Res Lett 40:1783–1788

Herrmann M, Somot S, Calmanti S, Dubois C, Sevault F (2011) Representation of spatial and temporal variability of daily wind speed and of intense wind events over the Mediterranean Sea using dynamical downscaling: impact of the regional climate model configuration. Nat Hazards Earth Syst Sci 11:1983–2001

Im ES, Coppola E, Giorgi F, Bi X (2010) Local effects of climate change over the Alpine region: a study with a high resolution regional climate model with a surrogate climate change scenario. Geophys Res Lett 37:L05704, doi: 10.1029/2009GL041801

Langner J, Engardt M Camilla A (2012) Modelling the impact of climate change on air pollution over Europe using the MATCH CTM linked to an ensemble of regional climate scenarios. In: Steyn DG, Trini Castelli S (eds) Air pollution modeling and its application XXI. Springer, Dordrecht, p 627–635

Laprise R, Kornic D, Rapai M, Šeparovi L and others (2012) Considerations of domain size and large-scale driving for nested regional climate models: impact on internal variability and ability at developing small-scale details. In: Berger A, Mesinger F, Sijacki D (eds) Climate change: inferences from paleoclimate and regional aspects. Springer, Vienna, p 181–199

Mariotti A, Dell'Aquila A (2012) Decadal climate variability in the Mediterranean region: roles of large-scale forcings and regional processes. Clim Dyn 38:1129–1145

Met Office Hadley Centre, Rayner NA, Parker D, Horton EB and others (2006) Met Office's global ice coverage and sea surface temperatures (GISST), and monthly night marine air temperature/SST anomalies (MOHMATN4)/(MOHSST6) data (1856–2006). NCAS British Atmospheric Data Centre. http://badc.nerc.ac.uk/data/gisst/ (accessed July 2011)

Önol B (2012) Effects of coastal topography on climate: high-resolution simulation with a regional climate model. Clim Res 52:159–174

Paeth H, Diederich M (2010) Postprocessing of simulated precipitation for impact research in West Africa. II. a weather generator for daily data. Clim Dyn 36:1337–1348

Pinto JG, Ulbrich S, Parodi A, Rudari R, Boni G, Ulbrich U (2013) Identification and ranking of extraordinary rainfall events over Northwest Italy: the role of Atlantic moisture. J Geophys Res Atmos 118:2085–2097

Rajczak J, Pall P, Schär C (2013) Projections of extreme precipitation events in regional climate simulations for Europe and the Alpine Region. J Geophys Res Atmos 118:3610–3626

Rauscher SA, Coppola E, Piani C, Giorgi F (2010) Resolution effects on regional climate model simulations of seasonal precipitation over Europe. Clim Dyn 35:685–711

Teutschbein C, Seibert J (2010) Regional climate models for hydrological impact studies at the catchment scale: a review of recent modeling strategies. Geogr Compass 4: 834–860

Toreti A, Desiato F, Fioravanti G, Perconti W (2010) Seasonal temperatures over Italy and their relationship with low-frequency atmospheric circulation patterns. Clim Change 99:211–227

Tramblay Y, Ruelland D, Somot S, Bouaicha R, Servat E (2013) High-resolution Med-CORDEX regional climate model simulations for hydrological impact studies: a first evaluation in Morocco. Hydrol Earth Syst Sci Discuss 10:5687–5737

Unal Y, Kindap T, Karaca M (2003) Redefining the climate zones of Turkey using cluster analysis. Int J Clim 23: 1045–1055

Uppala SM, Kållberg PW, Simmons AJ, and others, (2005) The ERA-40 re-analysis. QJR Meteorol Soc 131:2961–3012

Vrac M, Stein M, Hayhoe K (2007) Statistical downscaling of precipitation through nonhomogeneous stochastic weather typing. Clim Res 34:169–184

Ward JH Jr (1963) Hierarchical grouping to optimize an objective function. J Am Stat Assoc 58:236–244

White RH, Toumi R (2013) The limitations of bias correcting regional climate model inputs. Geophys Res Lett 40:2907–2912

Winterfeldt J, Geyer B, Weisse R (2011) Using QuikSCAT in the added value assessment of dynamically downscaled wind speed. Int J Climatol 31:1028–1039

Wilks DS (2011) Statistical methods in the atmospheric sciences, 3rd edn. Academic Press, Waltham, MA

WMO (1983) Guide to climatological practices WMO-No. 100 (3rd edn). www.wmo.ch/pages/prog/wcp/ccl/guide/guide_climat_practices.html

*Editorial responsibility: Filippo Giorgi, Trieste, Italy*

*Submitted: July 17, 2013; Accepted: July 25, 2014*
*Proofs received from author(s): January 26, 2015*